The structure of water at a Pt(111) electrode and the potential of zero charge studied from first principles

Sung Sakong,[1,*] Katrin Forster-Tonigold,[2] and Axel Groß[1,2,†]

[1] *Institute of Theoretical Chemistry, Ulm University, 89069 Ulm, Germany*
[2] *Helmholtz Institute Ulm (HIU), Electrochemical Energy Storage, 89069 Ulm, Germany*

The structure of a liquid water layer on Pt(111) has been studied by ab initio molecular dynamics simulations based on periodic density functional theory (DFT) calculations. First the reliability of the chosen exchange-correlation function has been validated by considering water clusters, bulk ice structures and bulk liquid water, confirming that the dispersion corrected RPBE-D3/zero functional is a suitable choice. The simulations at room temperature yield that a water layer that is six layers thick is sufficient to yield liquid water properties in the interior of the water film. Performing a statistical average along the trajectory, a mean work function of 4.88 V is derived giving a potential of zero charge of Pt(111) of 0.44 V vs. standard hydrogen electrode, in good agreement with experiments. Therefore we propose the RPBE-D3/zero functional as the appropriate choice for first-principles calculations addressing electrochemical aqueous electrolyte/metal electrode interfaces.

I. INTRODUCTION

Structures and processes at water/metal interfaces are of great technological importance [1–3], for example in electrochemical energy conversion and storage devices, electrocatalysis, or corrosion, just to name a few. From a theoretical point of view, a quantum chemical description of the water-metal interface is desirable, as the water-metal interaction influences the strength of the water-water interaction [4, 5]. However, the high computational cost of first-principles electronic structure calculations, even on the basis of density functional theory (DFT), still hampers the proper statistical description of metal-liquid water interfaces [6–8]. Furthermore, there are concerns as far as the reliability of current DFT exchange-correlation functionals for the water description are concerned [9, 10].

It is a well-known problem that widely used density functionals based on generalized gradient approximation (GGA), such as the popular Perdew-Becke-Ernzerhof (PBE) functional [11], lead to an over-structuring of liquid water [12, 13] compared to experiments [14] which is caused by the over-estimation of the directional hydrogen-bonding in the PBE functional [15]. Still the PBE functional has been used quite frequently to address properties of systems including liquid water [16–19]. In order to reproduce the structural properties of liquid water at room temperature correctly, the temperature in the molecular dynamics runs has been deliberately raised [16–18]. Of course, this is not a very satisfactory approach. The temperature correction is only appropriate for the simulations of pure bulk liquid water. When another species than water molecule is included into simulations, the temperature correction will produce wrong thermal properties of the additional species. Especially, when electrode-electrolyte interfaces are simulated, then the temperature correction cause a wrong population of vibrational states in the electrode and any adsorbates on the electrode.

Nuclear quantum effects [20, 21] are apparently not responsible for the over-structuring of PBE water as there are competing quantum effects that cancel to a large extent [22, 23]. Instead, it has been suggested that a proper handling of dispersion interactions in the water description might be crucial for a reliable description of water properties [19, 24–26]. However, in many of these studies hybrid DFT functional including exact exchange have been employed, but these functionals are not well-suited to describe metal-water interfaces as the inclusion of exact exchange in DFT functionals deteriorates the description of metals [27].

Recently we have demonstrated that the combination of a revised version of the PBE functional (RPBE [28]) together with dispersion correction suggested by Grimme *et al.* [29] yields a rather satisfactory description of the properties of liquid water [15]. The success of this RPBE-D3 scheme is caused by the fact that the overestimated directional hydrogen bonding existent in PBE is replaced by the non-directional van der Waals interaction. Not only the water-water interaction is appropriately adjusted by the consideration of dispersion effects, also the treatment of the water-metal interaction is improved resulting in a correct description of the wetting behavior of water on several metal surfaces [30–32].

We have now extended our previous studies concerning the proper first-principles description of the water-metal and water-water interaction [15, 30, 31]. This work is part of a long-standing project to model structures and processes at electrochemical metal electrode/aqueous electrolyte interfaces [4, 6–8, 33–38]. In electrochemistry, the electrode potential is a crucial quantity determining the structure of electrode/electrolyte interfaces [39]. The electrode potential is related to the workfunction of a metal in the presence of a liquid layer [40–46]. As water molecules have a sizable dipole moment, the workfunction of a water-covered metal electrode depends sen-

* sung.sakong@uni-ulm.de
† axel.gross@uni-ulm.de

sitively on the structure and orientation of the water molecules [7, 33, 47, 48], therefore a correct description of water-water and water-metal interactions is essential for reproducing electrochemical properties. Therefore, in this paper we first present an extended validation of the RPBE-D3 approach with respect to a proper structural description of isolated water clusters [10, 49, 50], bulk ice [26] and bulk water. In this context, we particularly focus on the role of the damping functions in the dispersion correction scheme, i.e., we compare results obtained with the Becke-Jonson (D3/bj) and zero (D3/zero) damping functions [29, 51].

Furthermore, we address an important electrochemical quantity, the potential of zero charge (pzc) which according to Trasatti is given by the workfunction of a metal covered by a pure, ion-free water film [41, 42, 48]. Experimentally, pzc of Pt(111) has been measured to be in the 4.8-4.9 V range in an absolute electrode potential scale [42, 45, 46, 52]. Theoretically, Tripkovic *et al.* tried to derive the pzc of several metal electrodes by selecting an appropriately chosen static water adsorption structure [48]. Here, we rather perform large scale AIMD simulations, making sure that we properly reproduce liquid water properties in the water film. Thus we obtain a value of the pzc in good agreement with the experiment, demonstrating that the RPBE-D3/zero approach is well-suited to describe metal electrode/aqueous electrolyte interfaces.

II. NUMERICAL METHODS

The periodic DFT calculations have been performed using the software package VASP [53]. The electronic cores are described by the projector augmented wave method [54] and the electronic one-particle states are expanded up to 400 eV using a plane wave basis set. Exchange-correlation effects have been taken into account within the generalized gradient approximation using the PBE [11] and the RPBE functionals [28]. Semi-empirical dispersion corrections have been taken into account according to Grimme's D3 scheme with both Becke-Jonson (D3/bj) and zero (D3/zero) damping functions [29, 51].

The small water clusters have been described in a cubic box of 17 Å^3 using just the the Gamma point in the k-point summation. Thus, the periodic images of clusters are separated by vacuum layers wider than 12 Å. The pairwise dispersion interactions are summed over the atoms with a cutoff radius of 10 Å, to avoid the contributions from periodic images. The bulk ice crystals are optimized based on the configurations obtained with the PBE functional [26]. To achieve a numerically stable optimization of the ice structures, the energy cutoff has been raised to 500 eV. A $2 \times 2 \times 2$ k-point grid has been used for the integration over the first Brillouin zone. The pairwise dispersion interactions have been summed within a radius of 50 Å. The numerical setup satisfies convergence criteria of 0.5 meV/H_2O with respect to the total energy and of 0.01 Å^3 with respect to the unit cell volume.

The thermodynamic properties of liquid water have been derived from ab initio molecular dynamics (AIMD) simulations with a time step of 1 fs performed at the Gamma k-point. The density of liquid water at 298 K (1g/cm^3) is emulated by 96 water molecules in a cubic cell of 14.2 Å^3. The equilibrium state of the canonical NVT ensemble at 298 K has been calculated by solving Langevin equation with a friction coefficient of $\gamma = 5\,\mathrm{ps}^{-1}$. The system has been thermalized for 10 ps, and the statistical sampling has been performed during the subsequent 30 ps run.

The water metal interface is modeled by 36 water molecules corresponding to six layers of water on a five-layer Pt(111) slab within a 3×3 unit cell. The integration over the first Brillouin zone is replaced by a summation over a 5×5 k-points. As the D3 dispersion correction scheme does not correctly describe the screening of the dispersion interaction within the bulk metal [30, 55], in the pairwise summation we only include the dispersion interaction between the Pt atoms of the top most layer and the water molecules as well as the dispersion interactions within/between water molecules. The pairwise dispersion interactions are summed over the atoms within a radius of 10 Å, to exclude interactions between water molecules and periodic images of the Pt layers. For bulk Pt, a lattice constant of 3.99 Å is obtained using a fine k-point grid of $21 \times 21 \times 21$ and the RPBE functional. The top three layers of the Pt slab are fully relaxed, while the bottom two layers are fixed at their bulk positions. The water film has a thickness of about 20 Å separated by 15 Å of vacuum from the next metal slab. The AIMD simulations for the Pt(111)-water interface have been performed using the same setup as for the bulk liquid water simulations. In addition, we have performed an extra 30 ps AIMD run with less tight energy convergence criteria to thermalize the water structure.

III. WATER-WATER INTERACTION WATER CLUSTER, BULK ICE AND BULK LIQUID WATER

In this section, we study the energetics and structure of small water clusters, bulk ice and bulk liquid water using the PBE and the RPBE functional. For RPBE, we additionally performed calculations in the D3 scheme with bj and zero damping. The results for the small clusters will be compared to those recently obtained using a coupled cluster method [50], and the calculations for bulk ice will be contrasted with experimental results that are extrapolated to zero temperature [56].

The formation energy of the water clusters and the bulk ice structure is referred to the isolated water molecule. Thus, the formation energy per water molecule is given by $E_\mathrm{f} = (E_\mathrm{cluster/ice} - nE_{\mathrm{H_2O}})/n$, where

$E_{\mathrm{cluster/ice}}$ is the total energy of water cluster/ice system, $E_{\mathrm{H_2O}}$ is the total energy of an isolated water molecule, and the number of water molecules in the cluster and the unit cell of the ice bulk structure, respectively, is denoted by n.

A. Small water clusters

In order to validate the reliability of the dispersion-corrected RPBE functional with respect to the modeling of small water cluster, we use coupled cluster CCSD(T) calculations performed by Temelso *et al.* [50] as a reference. These clusters contain up to ten water molecules. We have relaxed the CCSD(T) structures employing the RPBE, RPBE-D3/zero, RPBE-D3/bj, and PBE functionals. The 38 resulting cluster geometries obtained with the RPBE-D3/zero method are illustrated in Fig. 1. Note that we confirmed the CCSD(T) local minimum structures, except for the water-4-Py configuration marked by the diagonal dashed line in Fig. 1. This cluster converged to the water-4-Ci geometry In our DFT structure optimization for all considered GGA functionals.

The formation energies of the 38 water clusters according to the CCSD(T) calculations [50] and the deviations of the DFT-GGA values from the CCSD(T) results are listed in Table I. Note that the RPBE functional leads to an underestimation the cluster formation energies, whereas the PBE and the dispersion-corrected RPBE functionals cause a slight overestimation of the formation energies compared to the CCSD(T) results. For the water dimer that is denoted as the water-2-Cs configuration, the RPBE-D3/bj functional outperforms the RPBE-D3/zero functional, however, we are considering errors of only 1 and 2 meV, respectively, with regard to the CCSD(T) calculations. For all other larger water clusters, the results obtained with the RPBE-D3/zero functional are significantly closer to the CCSD(T) results than those calculated with the RPBE-D3/bj functional.

In total, for the RPBE-D3/zero functional a mean absolute deviation (MAD) from the CCSD(T) values of only 9 meV per H_2O molecule results. As Fig. 1 illustrates, the set of water clusters consists of rather different shapes and geometries, from more planar configurations to compact structures, also spanning a wide range of possible coordinations. The rather small MAD already indicates that the RPBE-D3/zero functional gives an accurate and reliable description of the water-water interaction. In contrast, the PBE functional yields a MAD of 34 meV/H_2O with respect to the CCSD(T) values that is about four times larger than the one according to the RPBE-D3/zero functional. When dispersion corrections are added to the PBE functional, then this error only becomes larger as dispersion leads to additional attractive interaction.

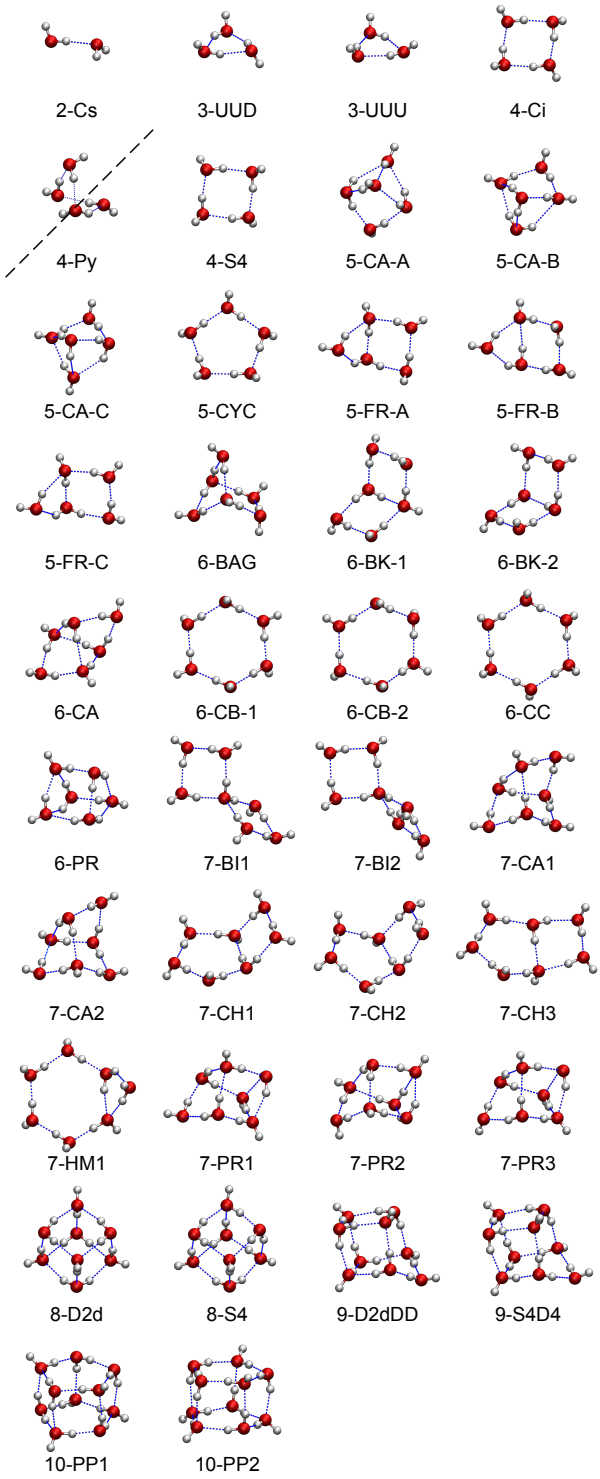

FIG. 1. Configuration of water clusters relaxed using the RPBE-D3/zero method. The initial structures were taken from recent CCSD(T) calculations [50]. Hydrogen bonds are indicated by dashed blue lines.

B. Ice structures

In addition to small water clusters, we also considered crystalline ice in our validation of the GGA functionals. In ice crystals, the water molecules are typically fully coordinated through hydrogen bonds, but the symmetry and water density can differ significantly. As far as the initial configurations are concerned, we start with the energy minimum structures obtained by Santra *et al.* using the PBE functional [26]. Both the geometry as well as the cell volume are optimized simultaneously. Figure 2 illustrates the equilibrium ice configurations obtained with the RPBE-D3/zero functional.

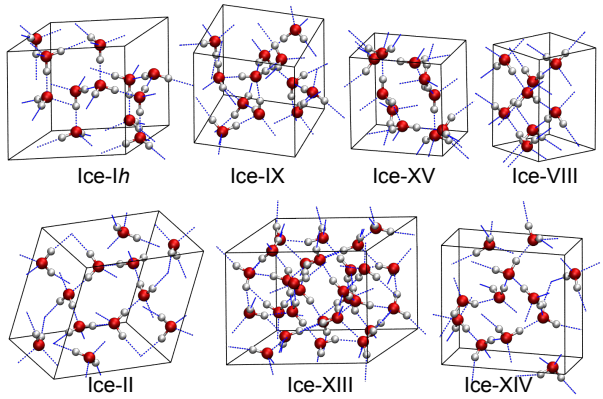

FIG. 2. Optimized ice crystal structures obtained with the RPBE-D3/zero functional. Blue dashed lines represent hydrogen bonds.

TABLE I. The formation energies of the small water clusters from CCSD(T) calculations (E_{ref}) taken from Ref. 50 and the deviation compared to E_{ref} in the calculations with RPBE, RPBE-D3/zero, RPBE-D3/bj, and PBE methods. The mean absolute deviation (MAD) shows that RPBE-D3/zero method reproduces the CCSD(T) calculations best.

	E_{ref} (eV/H_2O)	$E_{\mathrm{f}} - E_{\mathrm{ref}}$ (eV/H_2O)			
Water clusters	CCSD(T)	RPBE	D3/zero	D3/bj	PBE
Water-2-Cs	−0.109	0.023	−0.002	−0.001	−0.007
Water-3-UUD	−0.227	0.052	−0.004	−0.006	−0.020
Water-3-UUU	−0.218	0.054	−0.001	−0.002	−0.016
Water-4-Ci	−0.288	0.051	−0.007	−0.014	−0.036
Water-4-Py	−0.259		unstable		
Water-4-S4	−0.297	0.051	−0.008	−0.015	−0.037
Water-5-CA-A	−0.300	0.048	−0.008	−0.008	−0.041
Water-5-CA-B	−0.293	0.031	−0.012	−0.026	−0.051
Water-5-CA-C	−0.301	0.065	−0.009	−0.015	−0.030
Water-5-CYC	−0.312	0.048	−0.008	−0.016	−0.042
Water-5-FR-A	−0.287	0.058	−0.012	−0.015	−0.032
Water-5-FR-B	−0.303	0.051	−0.008	−0.011	−0.029
Water-5-FR-C	−0.281	0.056	−0.013	−0.016	−0.032
Water-6-BAG	−0.322	0.061	−0.011	−0.017	−0.036
Water-6-BK-1	−0.329	0.061	−0.009	−0.015	−0.037
Water-6-BK-2	−0.326	0.060	−0.010	−0.016	−0.037
Water-6-CA	−0.332	0.075	−0.008	−0.011	−0.026
Water-6-CB-1	−0.315	0.049	−0.007	−0.015	−0.041
Water-6-CB-2	−0.314	0.050	−0.006	−0.014	−0.040
Water-6-CC	−0.322	0.050	−0.006	−0.014	−0.041
Water-6-PR	−0.333	0.075	−0.008	−0.008	−0.021
Water-7-BI1	−0.331	0.059	−0.011	−0.018	−0.041
Water-7-BI2	−0.330	0.059	−0.010	−0.018	−0.040
Water-7-CA1	−0.345	0.070	−0.010	−0.016	−0.034
Water-7-CA2	−0.340	0.070	−0.010	−0.016	−0.034
Water-7-CH1	−0.337	0.058	−0.009	−0.017	−0.041
Water-7-CH2	−0.334	0.058	−0.010	−0.017	−0.040
Water-7-CH3	−0.329	0.060	−0.008	−0.014	−0.037
Water-7-HM1	−0.324	0.058	−0.006	−0.012	−0.036
Water-7-PR1	−0.355	0.077	−0.009	−0.013	−0.029
Water-7-PR2	−0.354	0.080	−0.009	−0.012	−0.028
Water-7-PR3	−0.352	0.078	−0.008	−0.012	−0.028
Water-8-D2d	−0.393	0.086	−0.011	−0.017	−0.035
Water-8-S4	−0.393	0.086	−0.010	−0.017	−0.035
Water-9-D2dDD	−0.394	0.080	−0.012	−0.019	−0.039
Water-9-S4DA	−0.392	0.080	−0.012	−0.019	−0.039
Water-10-PP1	−0.403	0.081	−0.013	−0.020	−0.040
Water-10-PP2	−0.403	0.081	−0.013	−0.020	−0.040
MAD		0.062	0.009	0.014	0.034

The experimentally determined values of the volume per water molecule extrapolated to zero temperature [56] are listed in Table II and compared to the theoretical results. Again, we find that the RPBE-D3/zero functional performs best among the considered functionals with a MAD of only 3.28 % compared to the experiment. Even more importantly, there is no outlier as far as the discrepancy with the experiment is concerned, which means that is describes all coordination patterns in the ice crystals equally well. The MAD obtained with the PBE and RPBE-D3/bj functionals of 3.44 % and 4.44 %, respectively, are also acceptable, however, they strongly underestimate the Ice-Ih volume. This implies that the PBE and RPBE-D3/bj functionals reproduce the properties of hydrogen bonds in different high coordination situations with a varying accuracy. Finally, the RPBE functional

TABLE II. Experimentally determined volumes of ice structures per water molecule compared to the calculated values obtained with the RPBE, RPBE-D3/zero, RPBE-D3/bj, and PBE functionals.

	V_{ref} (Å^3/H_2O)	$V/V_{\mathrm{ref}} - 1$ (%/H_2O)			
Ice crystals	Experiments	RPBE	D3/zero	D3/bj	PBE
Ice-Ih	32.05	1.78	−3.88	−6.21	−7.71
Ice-IX	25.63	12.91	−2.29	−3.53	−1.48
Ice-II	24.97	11.09	−2.88	−4.08	−3.56
Ice-XIII	23.91	11.38	−2.90	−4.21	−3.51
Ice-XIV	23.12	12.11	−2.97	−4.54	−3.72
Ice-XV	22.53	13.80	−2.86	−3.94	−2.89
Ice-VIII	20.09	20.06	−5.18	−4.58	−1.19
MAD		11.88	3.28	4.44	3.44

leads to a large overestimation of the ice crystal volumes, or in other words, to a significant underestimation of the density of the ice structures.

The findings with respect to the ice volume are confirmed when the formation energies of ice crystals are considered, as Table III demonstrates. Again, the RPBE-D3/zero functional reproduces the experimental results [56] with the smallest MAD. Note that the MAD of 10 meV/H_2O in the formation energy of the ice crystals is comparable to the MAD of 9 meV/H_2O for the cluster calculations. This shows that the RPBE-D3/zero functionals describes finite and periodic water structures equally well. In contrast, the MAD for the RPBE, RPBE-D3/bj, and PBE bulk ice calculations is larger than the corresponding MAD for the cluster calculations, in particular for RPBE. This means that the RPBE, RPBE-D3/bj, and PBE functionals describe the high-coordinated bulk ice configurations with a lower accuracy than the cluster configurations which is disadvantageous with respect to the simulation of liquid water properties which requires a similar accuracy for all possible water configurations.

C. Thermodynamic properties of bulk liquid water

Finally, we checked the performance of the considered GGA functionals with respect to the simulation of bulk liquid water. The calculations have been performed in the canonical ensemble using the Langevin equation including 96 water molecules in the unit cell. A friction constant of $\gamma = 5\,\mathrm{ps}^{-1}$ has been selected to mimic the diffusive behavior of liquid water as suggested by Paterlini and Ferguson [57]. The NVT ensemble was equilibrated during the first 10 ps of the AIMD runs at 298 K. After then, the statistical sampling has been performed for the subsequent 30 ps. The temperature along the production runs satisfied a Gaussian distribution $\sim \exp[-(T-\mu)/2\sigma^2]$ with mean temperatures of $\mu =$ 297, 299, 297, and 300 K for the RPBE, RPBE-D3/zero, RPBE-D3/bj, and PBE functionals, respectively, and a variation of $\sigma = 14$ K for all functionals. Hence, the sampling of the this canonical ensemble is appropriate to derive equilibrium water properties.

TABLE III. Experimentally derived formation energies of ice crystal [56] compared to the calculated results obtained with the RPBE, RPBE-D3/zero, RPBE-D3/bj, and PBE functionals.

	E_{ref} (eV/H_2O)	$E_{\mathrm{f}} - E_{\mathrm{ref}}$ (eV/H_2O)			
Ice crystals	Experiments	RPBE	D3/zero	D3/bj	PBE
Ice-Ih	−0.610	0.122	−0.027	−0.043	−0.054
Ice-IX	−0.606	0.160	−0.010	−0.023	−0.011
Ice-II	−0.609	0.195	−0.002	−0.006	0.016
Ice-VIII	−0.577	0.282	0.003	0.033	0.101
MAD		0.190	0.011	0.026	0.046

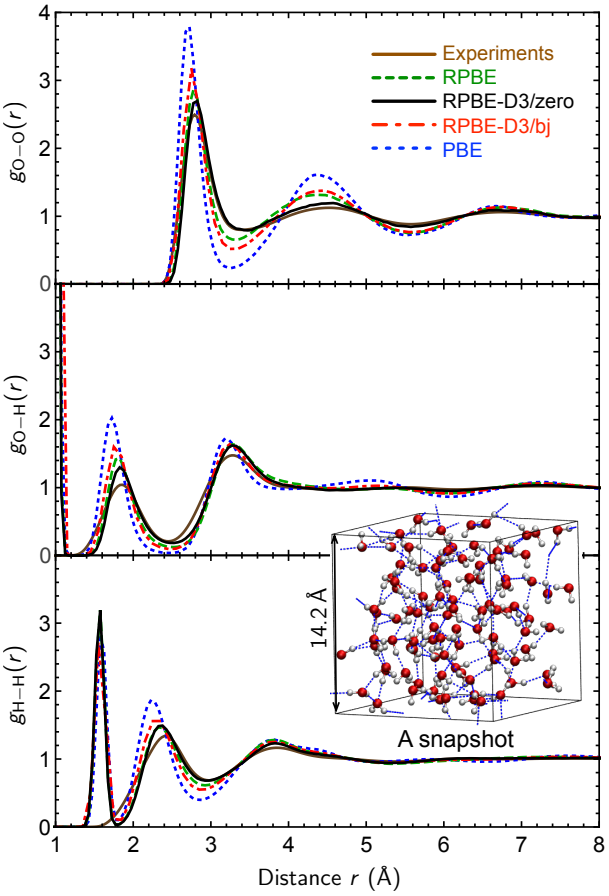

FIG. 3. Radial distribution functions of atom A and B $g_{A-B}(r)$ in liquid water simulations are compared to neutron scattering experiments.

In Fig. 3, the calculated radial distribution functions for the various functionals are compared to the results of neutron scattering experiments by Soper [14]. As already shown in a previous study with a smaller unit cell [15], the RPBE-D3/zero functional reproduces the radial distribution functions of liquid water most closely among the considered functionals, as a visual inspection of Fig. 3 reveals. In order to quantify the discrepancy between theory and experiment, we evaluated the integral $\int |g_{O-O}(r') - g^{\mathrm{exp}}_{O-O}(r')|dr'$ and normalized it to the number of water molecules by unit cell. This error measure yields values of 0.6, 0.3, 0.7, 1.4 for the RPBE, RPBE-D3/zero, RPBE-D3/bj, and PBE functionals, respectively, verifying the visual impression. Note that the larger error in the PBE and RPBE-D3/bj calculations is related to the existence of the peaks in the $g_{O-O}(r)$ distribution which are too much pronounced indicating an over-structuring of the simulated liquid.

Note that the reliability of any water simulation is closely related to the fact how well the hydrogen bonds

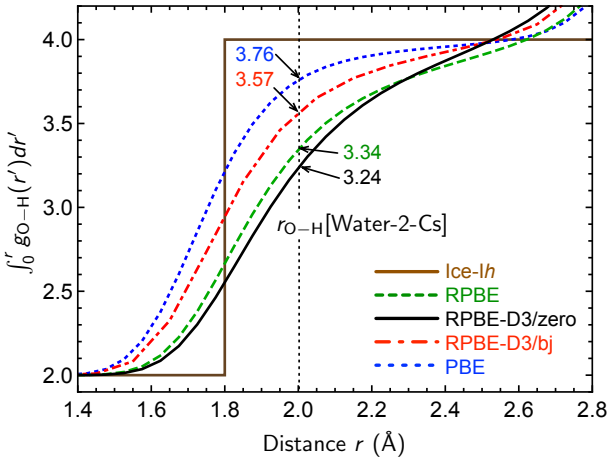

FIG. 4. Integrated radial O-H distribution functions $\int_0^r g_{O-H}(r')dr'$ as a function of the upper boundary for Ice-Ih and liquid water simulations using GGA functionals.

are described. In the following we will focus on the coordination of liquid water, i.e., on the average number of hydrogen bonds per water molecules. Experimentally, an average number of 3.3 hydrogen bonds per molecule in liquid water has been derived from X-ray adsorption spectroscopy [58–60]. For simplicity, we identify the number of hydrogen bonds by the probability that O-H bonds of a certain distance occur. Then, the number of hydrogen bonds can be estimated from the integral over the radial distribution function $g_{O-H}(r)$ up to a given distance. The corresponding integrals as a function of the upper boundary obtained with the four different functionals are plotted in Fig. 4. In addition, the corresponding curve for Ice-Ih is plotted. The second nearest-neighbor O-H distance in Ice-Ih corresponding to the O-H distance in hydrogen bonds is 1.8 Å. Consequently, the integral over the radial distribution function jumps from two for the two O-H bonds within a water molecule to four at this value in a step-function like fashion.

In liquid water, however, the integral over $g_{O-H}(r)$ is a smooth continuous function. Typically, hydrogen bonds are assumed to have a length between 1.6 and 2.0,Å. Therefore we have selected 2.0,Å as the upper value in the integrals in order to determine the water coordination, indicated by the dashed line in Fig. 4. Admittedly, this choice is somewhat arbitrary, but the general trends should be independent of this particular value. Thus we obtain effective coordination numbers of 3.34, 3.24, 3.57, and 3.76 in the liquid water simulations performed with the RPBE, RPBE-D3/zero, RPBE-D3/bj, and PBE functionals, respectively. The results for the RPBE and RPBE-D3/zero functionals match the results of the spectroscopy experiments considerably well, whereas the RPBE-D3/bj and PBE functionals overestimate the water coordination. In particular, the estimated coordination of PBE water of 3.76 is too close to the ice-like coordination of 4. This confirms the well-known fact that PBE leads of an over-structuring of liquid water.

In spite of the good estimation of the water coordination, the RPBE functional still does not yield a satisfactory description of water properties. As shown in Fig. 4, RPBE water reaches a coordination of 4 at a larger value than all other functionals. As a consequence, the equilibrium density of RPBE water too low. Therefore, RPBE water is slightly compressed in the chosen unit cell corresponding to a water density of 1g/cm^3. This result is consistent with the overestimated equilibrium volumes of the ice crystals derived from RPBE calculations (see Table II).

Summarizing the results of this section, the RPBE-D3/zero functional yields a satisfactory description the properties of water cluster, bulk ice crystals and bulk liquid water indicating that the water-water interaction is well reproduced in this particular approach.

IV. THERMODYNAMICS OF THE Pt(111)-LIQUID WATER INTERFACE

In the previous section we have confirmed that the RPBE-D3/zero functional is well-suited to reproduce the properties of water systems. In addition, in previous studies we have already shown that the RPBE-D3/zero functional also yields a reliable description of the water-metal interaction. It reproduces the right wetting behavior of water on various metal surfaces [30], whereas RPBE, PBE and dispersion-corrected PBE calculations fail to predict this correctly. Therefore, the RPBE-D3/zero functional represents the optimal choice to address properties of aqueous electrolyte-electrode interfaces from first principles.

There has been a long debate whether water layers at closed-packed metal surfaces are ice-like or not. AIMD simulations have indicated that already the first water layer on fcc(111) metal surfaces is disordered, at least as far as the orientation of the water molecules is concerned [7]. Still it is not clear at which distance from the metal surface water really becomes bulk water liquid-like. In order to address this issue, we have considered a relatively thick water layer on a Pt(111) slab still taking vacuum above the water into account. This will also allow us to derive the potential of zero charge of the Pt(111) electrode. In detail, we have selected a 3×3 surface unit cell of Pt(111) covered by 36 water molecules leading to a water layer with a thickness of about 20 Å roughly corresponding to six bilayers of water. This water layer is separated by a vacuum layer of 15 Å thickness from the bottom of the next metal slab.

A. Thermodynamic equilibrium of electrode and electrolyte

The thermodynamic sampling has been performed with solving the Langevin equation at 298 K. We start

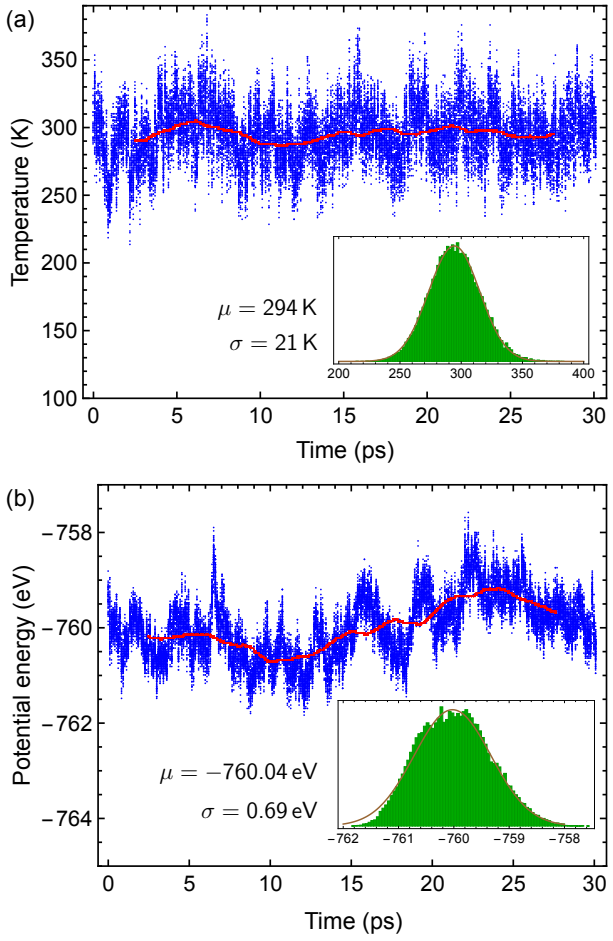

FIG. 5. Calculated values of (a) the temperature and (b) the potential energy of the liquid water-Pt(111) interface along the AIMD trajectory. The red dots correspond to values averaged over 5 ps. In the insets, the distribution in the temperature and potential energy are shown together with Gaussian fits.

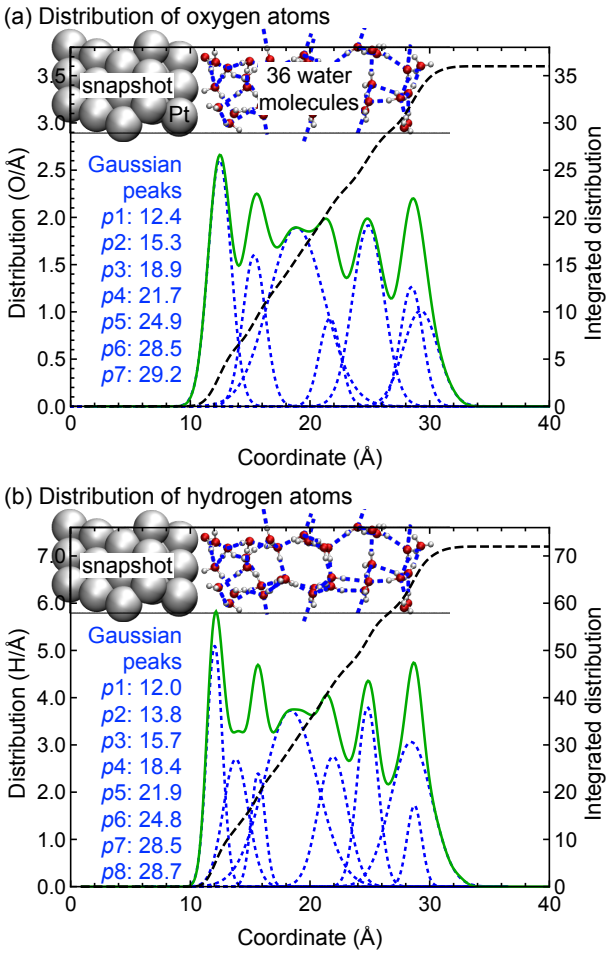

FIG. 6. Mean value along the AIMD runs of the laterally averaged distribution of (a) the oxygen and (b) the hydrogen atoms of the water molecules as a function of the distance from the surface (green solid lines) together with a deconvolution in terms of Gaussian functions (blue short-dashed lines). The long-dashed black lines show the integrated distributions.

from a bulk liquid configuration placed on metal electrode. We bring the water configuration at the interface and the surface close to the equilibrium during 30 ps with less tight energy convergence. After then, the energy convergence is switched to the production accuracy. The system is thermalized during 10 ps and the thermodynamic sampling is performed during 30 ps with RPBE-D3/zero method.

Figure 5 presents the temperature derived from the kinetic energy and the potential energy along the 30 ps production runs. The red lines correspond to values averaged over 5 ps. The insets of Fig. 5 illustrate the distribution of temperature and potential energy together with Gaussian fits, the corresponding fit parameters are given in the two panels. There is some long-time oscillation in the potential energy. Still, both the temperature and the potential energy follow a Gaussian distribution indicating an appropriate sampling within a canonical ensemble. This allows to derive equilibrium properties of the electrode-electrolyte interface from the AIMD runs. Note that the mean temperature of the system is $\mu = 294\,\mathrm{K}$ with a variation of $\sigma = 21\,\mathrm{K}$. No water dissociation has been observed during the simulation time.

B. Spatial distribution of water molecules at the electrode-electrolyte interface

In order to analyze the structure of the water layer, we have plotted the mean value along the AIMD runs of the laterally averaged distribution of the hydrogen and oxygen atoms of the water molecules as a function of the distance from the surface in Fig. 6 together with a deconvolution in terms of Gaussian functions. In addition, the integrated distributions are shown. Note that

the integrated distributions corresponds to straight lines in the interior part of the water layer for z-values of $14 < z < 26$ Å). This indicates that there is no pronounced layer structure in the middle of the water layers, or in other words, that the distribution of water molecules corresponds to a liquid state. This conclusion is supported by the estimated density of water molecules in $12 < z < 29$ Å which corresponds to the bulk liquid water value of 1.0 g/cm^3 at 298 K.

We are now analyzing the spatial distribution and orientation of the water molecules in more detail. The oxygen distribution peak directly at the interface ($p1$ in Fig. 6a) corresponds to about six oxygen atoms. The water coordination at the interface is in fact the same as in ice-like water bilayers on metal surfaces. The related hydrogen distribution peak ($p1$ in Fig. 6b) contains around 11 hydrogen atoms. Note that the positions of the $p1$-oxygen and the $p1$-hydrogen peak are almost same. This means that there is no preferred orientation of the water hydroxyl bond with respect to the direction normal to the surfaces, i.e., there is no preference for either the H-up of the H-down water structure. This confirms the findings of a previous AIMD study of water layers on metal surfaces [7].

Focusing on the water-vacuum interface, there are two oxygen distribution peaks ($p6$ and $p7$ in Fig. 6a) consisting of three atoms each at the water-vacuum interface consist of three atoms. At the same height there is also a pronounced peak in the hydrogen distribution ($p7$ and $p8$ in Fig. 6b). This shows that there is also no preferred water orientation of the water O-H bonds perpendicular to the water-vacuum interface.

C. Potential of zero charge of Pt(111) electrode

Finally, we address the potential of zero charge (pzc) of the Pt(111) electrode. According to Trasatti [42], the potential of zero charge of a metal electrode can be derived from the work function of the metal covered with an ion-free water film. This definition has also been used in the DFT study of Tripkovic *et al.* [48]. We have collected the work function at each MD step as shown in Fig. 7. It has been evaluated by the difference between the the Fermi level and the vacuum level which is estimated from the electrostatic one-electron potential including dipole corrections to account for the asymmetry in the vertical direction. There seems to be a drift of the work function along the trajectory which might be related to the observed structure in the potential energy as a function of run time (see Fig. 5b). Still, the distribution of the work function is Gaussian-like (see the inset of Fig. 7) which is consistent with a canonical ensemble.

The mean work function of the trajectory is 4.88 V which is in nice agreement with the measured absolute pzc of 4.9 V derived using the CO adsorption technique [42, 45, 46, 52]. When we take the value of of 4.44 V for the absolute standard hydrogen electrode (SHE) potential which is suggested by both theory and experiments [40, 41, 48, 61], then the calculated pzc corresponds to 0.44 V versus SHE.

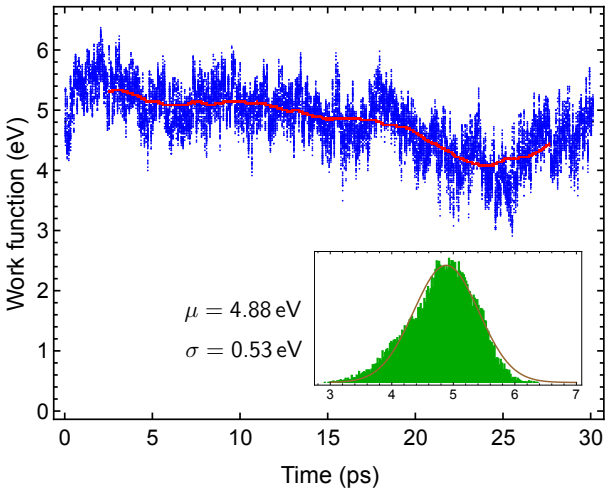

FIG. 7. Calculated work function of the water-covered Pt(111) slab along the AIMD trajectory. The red dots correspond to values averaged over 5 ps. In the inset, the distribution in the work function is shown together with a Gaussian fit.

Note that the work function of a water/metal system includes contributions from the dipole moments at the solvated metal electrode surface and the averaged dipole moments of liquid water along the surface normal. These averaged dipole moments are related to the equilibrium distribution in the orientation of water molecules in the liquid water film. The fact that the RPBE-D3/zero calculations are able to predict the correct potential of zero charge of Pt(111) indicates that the RPBE-D3/zero functional is suitable to describe the atomic structure and electronic distribution within the electric double layer. Furthermore, our results indicate that a water film with a thickness of 20 Å should be sufficient to model the electric double layer.

V. CONCLUSIONS

Calculating the properties of water clusters, bulk ice crystals and bulk liquid water with total energy electronic structure calculations based on density functional theory, we have confirmed that the RPBE-D3/zero functional yields a reliable description of the water-water interaction. We have then used this functional to study the properties of a water film with a thickness of 20 Å on a Pt(111) electrode by performing ab initio molecular dynamics simulations at room temperature. It turns out that the water is bulk-liquid like in the interior of the water film. Furthermore, by taking the average work function along the trajectory, a potential of zero charge of 4.88 V corresponding to 0.44 V versus SHE has

been derived in good agreement with experiments. This demonstrates first that the RPBE-D3/zero functional is a good choice to address electrochemical interfaces between a metal electrode and an aqueous electrolyte from first principles, and second, that a 20 Å thick water film should be sufficient to model the electric double layer at these interfaces.

ACKNOWLEDGEMENT

This research has been supported by the German Research Foundation (DFG) through the research unit FOR 1376 (DFG contract GR 1503/21-1) and by the Baden-Württemberg Foundation within the Network of Excellence Functional Nanostructures. Computer time on the JUSTUS cluster at Ulm University has been provided by the bwHPC initiative and the bwHPC-C5 project which are funded by the Baden-Württemberg government (MWK) and the German Research Foundation (DFG).

[1] R. Guidelli and W. Schmickler, Electrochim. Acta **45**, 2317 (2000).
[2] A. Hodgson and S. Haq, Surf. Sci. Rep. **64**, 381 (2009).
[3] J. Carrasco, A. Hodgson, and A. Michaelides, Nat. Mater. **11**, 667 (2012).
[4] A. Roudgar and A. Groß, Chem. Phys. Lett. **409**, 157 (2005).
[5] A. Michaelides, Appl. Phys. A **85**, 415 (2006).
[6] A. Groß, F. Gossenberger, X. Lin, M. Naderian, S. Sakong, and T. Roman, Journal of The Electrochemical Society **161**, E3015 (2014).
[7] S. Schnur and A. Groß, New Journal of Physics **11**, 125003 (2009).
[8] X. Lin and A. Groß, Surf. Sci. **606**, 886 (2012).
[9] B. Santra, A. Michaelides, and M. Scheffler, J. Chem. Phys. **127**, 184104 (2007).
[10] B. Santra, A. Michaelides, M. Fuchs, A. Tkatchenko, C. Filippi, and M. Scheffler, The Journal of Chemical Physics **129**, 194111 (2008).
[11] J. P. Perdew, K. Burke, and M. Ernzerhof, Phys. Rev. Lett. **77**, 3865 (1996).
[12] J. C. Grossman, E. Schwegler, E. W. Draeger, F. Gygi, and G. Galli, J. Chem. Phys. **120**, 300 (2004).
[13] P. H.-L. Sit and N. Marzari, The Journal of Chemical Physics **122**, 204510 (2005).
[14] A. K. Soper, ISRN Physical Chemistry **2013**, 67 (2013).
[15] K. Forster-Tonigold and A. Groß, J. Chem. Phys. **141**, 064501 (2014).
[16] J. VandeVondele, F. Mohamed, M. Krack, J. Hutter, M. Sprik, and M. Parrinello, J. Chem. Phys. **122**, 014515 (2005).
[17] R. A. DiStasio, B. Santra, Z. Li, X. Wu, and R. Car, The Journal of Chemical Physics **141**, 084502 (2014).
[18] L. S. Pedroza, A. Poissier, and M.-V. Fernández-Serra, The Journal of Chemical Physics **142**, 034706 (2015).
[19] J. Wang, G. Román-Pérez, J. M. Soler, E. Artacho, and M.-V. Fernández-Serra, The Journal of Chemical Physics **134**, 024516 (2011).
[20] A. Groß and M. Scheffler, J. Vac. Sci. Technol. A **15**, 1624 (1997).
[21] A. Groß, J. Chem. Phys. **110**, 8696 (1999).
[22] S. Habershon, T. E. Markland, and D. E. Manolopoulos, J. Chem. Phys. **131**, 024501 (2009).
[23] S. Fritsch, R. Potestio, D. Donadio, and K. Kremer, J. Chem. Theory Comput. **10**, 816 (2014).
[24] C. Zhang, J. Wu, G. Galli, and F. Gygi, J. Chem. Theory Comput. **7**, 3054 (2011).
[25] J. Klimes and A. Michaelides, J. Chem. Phys. **137**, 120901 (2012).
[26] B. Santra, J. Klimeš, A. Tkatchenko, D. Alfè, B. Slater, A. Michaelides, R. Car, and M. Scheffler, The Journal of Chemical Physics **139**, 154702 (2013).
[27] J. Paier, M. Marsman, and G. Kresse, J. Chem. Phys. **127**, 024103 (2007).
[28] B. Hammer, L. B. Hansen, and J. K. Nørskov, Phys. Rev. B **59**, 7413 (1999).
[29] S. Grimme, J. Antony, S. Ehrlich, and H. Krieg, J. Chem. Phys. **132**, 154104 (2010).
[30] K. Tonigold and A. Groß, J. Comp. Chem. **33**, 695 (2012).
[31] S. Sakong, M. Naderian, K. Mathew, R. G. Hennig, and A. Groß, J. Chem. Phys. **142**, 234107 (2015).
[32] J. Carrasco, B. Santra, J. Klimeč, and A. Michaelides, Phys. Rev. Lett. **106**, 026101 (2011).
[33] S. Schnur and A. Groß, Catal. Today **165**, 129 (2011).
[34] T. Roman and A. Groß, Catal. Today **202**, 183 (2013).
[35] T. Roman and A. Groß, Phys. Rev. Lett. **110**, 156804 (2013).
[36] F. Gossenberger, T. Roman, K. Forster-Tonigold, and A. Groß, Beilstein J. Nanotechnol. **5**, 152 (2014).
[37] F. Gossenberger, T. Roman, and A. Groß, Surf. Sci. **631**, 17 (2015).
[38] N. G. Hörmann, M. Jäckle, F. Gossenberger, T. Roman, K. Forster-Tonigold, M. Naderian, S. Sakong, and A. Groß, J. Power Sources **275**, 531 (2015).
[39] W. Schmickler and E. Santos, *Interfacial electrochemistry*, Springer Berlin / Heidelberg, second edition, 2010.
[40] S. Trasatti, Journal of Electroanalytical Chemistry and Interfacial Electrochemistry **150**, 1 (1983).
[41] T. S., Pure and Applied Chemistry **58**, 955 (1986).
[42] S. Trasatti, Electrochimica Acta **36**, 1659 (1991).
[43] T. Pajkossy and D. Kolb, Electrochimica Acta **46**, 3063 (2001).
[44] V. Climent, B. A. Coles, , and R. G. Compton, The Journal of Physical Chemistry B **106**, 5988 (2002).
[45] A. Cuesta, Surface Science **572**, 11 (2004).
[46] O. A. Petrii, Russian Journal of Electrochemistry **49**, 401 (2013).
[47] J. S. Filhol and M.-L. Bocquet, Chem. Phys. Lett. **438**, 203 (2007).

[48] V. Tripkovic, M. E. Björketun, E. Skúlason, and J. Rossmeisl, Phys. Rev. B **84**, 115452 (2011).
[49] B. Santra, A. Michaelides, and M. Scheffler, The Journal of Chemical Physics **131**, 124509 (2009).
[50] B. Temelso, K. A. Archer, and G. C. Shields, The Journal of Physical Chemistry A **115**, 12034 (2011).
[51] S. Grimme, Wiley Interdisciplinary Reviews: Computational Molecular Science **1**, 211 (2011).
[52] M. J. Weaver, Langmuir **14**, 3932 (1998).
[53] G. Kresse and J. Furthmüller, Phys. Rev. B **54**, 11169 (1996).
[54] P. E. Blöchl, Phys. Rev. B **50**, 17953 (1994).
[55] G. Mercurio et al., Phys. Rev. Lett. **104**, 036102 (2010).
[56] E. Whalley, The Journal of Chemical Physics **81**, 4087 (1984).
[57] M. Paterlini and D. M. Ferguson, Chemical Physics **236**, 243 (1998).
[58] J. D. Smith, C. D. Cappa, K. R. Wilson, B. M. Messer, R. C. Cohen, and R. J. Saykally, Science **306**, 851 (2004).
[59] J. D. Smith, C. D. Cappa, B. M. Messer, R. C. Cohen, and R. J. Saykally, Science **308**, 793 (2005).
[60] A. Rastogi, A. K. Ghosh, and S. Suresh, *Hydrogen Bond Interactions Between Water Molecules in Bulk Liquid, Near Electrode Surfaces and Around Ions*, chapter 13, pages 351–364, Thermodynamics - Physical Chemistry of Aqueous Systems, InTech, 2011.
[61] H. Reiss and A. Heller, The Journal of Physical Chemistry **89**, 4207 (1985).